BRAIN CONNECTIVITY
Volume XX, Number XX, 2016

DOI: 10.1089/brain.2015.0392

ORIGINAL ARTICLE

Salience Network Activity in Perceptual Decisions

Bidhan Lamichhane,[1] Bhim M. Adhikari,[1] and Mukesh Dhamala[1–3]

Abstract

The dorsal anterior cingulate cortex (dACC) and the anterior insulae (AIs) are coactivated in various perceptual decision-making (PDM) tasks and form the salience network (SN): a key network in sensory perception and the coordination of behavioral responses. However, what the functional role of SN is, how these key SN nodes interact with each other to form a network in a perceptual decision, and how the network depends on the perceptual difficulty remain largely unknown. In the present study, we measured blood oxygen level-dependent (BOLD) signals using functional magnetic resonance imaging (fMRI). During four PDM tasks (1) face–house discrimination, (2) happy–angry face discrimination, (3) audiovisual asynchrony and synchrony perception, and a (4) random dot motion direction task, we varied the task difficulty and examined the interactions between these SN nodes. In all the experiments, behavioral accuracy decreased and response time increased with task difficulty. The BOLD signal increased in SN nodes with the ambiguity in the sensory information. We also found that there were significant directed functional connections between AIs and dACC in all four tasks and that the interactions between these nodes increased with task difficulty. The observed difficulty-dependent functional architecture of SN suggests that the dACC and AIs are part of a large-scale cognitive system that facilitates sensory integration in PDM.

Key words: anterior insulae; dorsal anterior cingulate cortex; functional magnetic resonance imaging; salience network; task difficulty

Introduction

The dorsal anterior cingulate cortex (dACC) and the anterior insulae (AIs) were found coactivated in neuroimaging studies on various perceptual decision-making (PDM) tasks (Binder et al., 2004; Bushara et al., 2001; Dosenbach et al., 2007; Ham et al., 2013; Lewis et al., 2000; Ploran et al., 2007; Tregellas et al., 2006). Together, the AIs and dACC form the ''salience'' network (SN) (Seeley et al., 2007; Sridharan et al., 2008), whose role in decision-making process includes implementation of goal-directed tasks (Dosenbach et al., 2006, 2007) and the coordination of behavioral responses (Medford and Critchley, 2010). We recently found that in a cognitively demanding goal-directed task, AIs appeared to be involved in integrating information and driving dACC guidance of response selection (Lamichhane and Dhamala, 2015b).

The dACC has long been implicated as a motor region due to its activation during movement (Paus, 2001; Picard and Strick, 1996). The dACC is also known to be associated with goal-directed action selection (Dosenbach et al., 2007; Medford and Critchley, 2010; Zysset et al., 2006). For example, dACC is found activated in reward-based action selection (Holroyd and Yeung, 2012; Rushworth et al., 2007). Lesions of dACC can hinder initiation of complex voluntary movements and actions (Rushworth et al., 2004; Williams et al., 2004) and cause increased and more variable response times (RT) in humans (Stuss et al., 2005), and cingulotomy patients usually recover most of these functions (Dougherty et al., 2002). In nonhuman primates, lesions result in impaired attention to task demands and disrupted task switching (Rushworth et al., 2003). Moreover, a recent study found that lesions of the white matter bundles projecting to and from dACC resulted in poor task performance (Metzler-Baddeley et al., 2012). Effects are due to the dACC role in top–down modulation of primary motor cortex (Taylor et al., 2007).

The AIs have been shown to be involved in cross-modal perceptual integration (Bushara et al., 2001; Chang et al., 2013; Ho et al., 2009; Lewis et al., 2000; Sterzer and Kleinschmidt, 2010). In addition, the blood oxygen level-dependent (BOLD) activity in AIs has been found correlated with difficulty of sensory cues in a PDM task (Lamichhane and Dhamala, 2015b). When the ambiguity in sensory information increased, this would increase the task difficulty level

[1]Department of Physics and Astronomy and [2]Neuroscience Institute, Georgia State University, Atlanta, Georgia.
[3]Center for Behavioral Neuroscience, Center for Nano-Optics, Center for Diagnostics and Therapeutics, Georgia State University, Atlanta, Georgia.

and people would be uncertain for selecting and deciding the appropriate action (Ho et al., 2009; Shenhav et al., 2013; Woolgar et al., 2011). For optimal performance, such uncertainty must be resolved (Botvinick et al., 2001), such as through AI integration of choice and guide dACC to choose appropriate behavior (Ho et al., 2009; Krebs et al., 2012; Rushworth et al., 2004; Srinivasan et al., 2013; Venkatraman et al., 2009; Wiech et al., 2010; Woolgar et al., 2011).

In this study, participants underwent functional magnetic resonance imaging (fMRI) while completing four PDM tasks: (1) face–house discrimination, (2) happy–angry face discrimination, (3) audiovisual asynchrony and synchrony perception task, and a (4) random dot motion (RDM) direction task. Here, task 3 involves both audio and visual stimuli, which provides us the opportunity to examine and explore the PDM in multi (bi-) sensory domain, whereas other three tasks involve only visual stimuli. These altogether allows us to investigate general brain mechanisms for decision-making across a wide range of tasks with different stimulus types and features. These four tasks were commonly used in the past decade to investigate PDM processes in the brain and all of the tasks involve decisions about two alternative choices and stimulus-noise-dependent behavioral performance variations. Across all of these tasks, we aimed to uncover the existence of a common network pattern for PDM and the network activity changes as a function of task difficulty. The rationale of difficulty manipulation is to examine how the noise level in stimuli influences nodal activity and network interactions among the nodes of SN. A recent work (Lamichhane and Dhamala, 2015b) showed that the activity of SN nodes is positively correlated with task difficulty. An increased engagement of SN in difficult task was proposed as neural signature of higher effort in sensory integration salience to task at hand (see Ham et al. (2013)) for a different opinion]. This finding prompted a question: is the SN functional architecture dependent on task difficulty? If so, how are nodes of the SN engaged to form perceptual decisions? We predicted a higher node and network-level activity within SN as required for stimulus salience integration in choosing appropriate motor command caused by ambiguity in sensory information (Ho et al., 2009; Krebs et al., 2012; Rushworth et al., 2004; Shenhav et al., 2013; Srinivasan et al., 2013; Venkatraman et al., 2009; Wiech et al., 2010; Woolgar et al., 2011). In addition to the findings of previous studies on the insula, a key structure in PDM (Binder et al., 2004; Grinband et al., 2006; Ho et al., 2009; Ploran et al., 2007; Tregellas et al., 2006) and a cortical ''out flow hub'' to influence dACC activity (Ham et al., 2013; Menon and Uddin, 2010; Sridharan et al., 2008), we aimed to provide additional evidence on its role in sensory integration and sensory motor mapping in coupling to dACC, a region known to have a major role in motor selection. Moreover, we explored how network interactions are modulated by decision difficulty across a variety of perceptual tasks in moment-to-moment integration of sensory information in PDM.

Materials and Methods

Participants

There were 32 human participants (16 males, 16 females; mean age ± standard deviation = 27.6 ± 4.7 years) who completed all four experimental tasks: (1) face–house discrimination, (2) happy–angry face discrimination, (3) audiovisual asynchrony/synchrony perception, and (4) an RDM direction discrimination task. One more male participant took part in face–house discrimination and in audiovisual asynchrony and synchrony perception tasks. Each participant visited for two MR scanning sessions on 2 different days within a 7-day period. Participants completed tasks 1 and 3 in the first visit, and tasks 2 and 4 in the second visit. Both behavioral data (performance accuracy) and fMRI data associated with the corresponding tasks were all collected. Behavioral data (performance accuracy and RTs) were collected outside the scanner first, and then, the behavioral data (performance accuracy) and brain data were collected inside the scanner. All participants had normal or corrected to normal vision and reported normal neurological history. No participant reported difficulties recognizing red and green dots during practice session hence no red/green color blindness was reported. Participants provided written signed informed consent forms and were compensated for their participation in the experiments. Institutional Review Board for Joint Georgia State University and Georgia Institute of Technology Center for Advanced Brain Imaging, Atlanta, Georgia, approved these studies.

Stimuli

Experiment 1: face–house discrimination task. In the face–house discrimination task, a total of 14 images of faces and 14 images of houses were downloaded from F.A.C.E. Training—an interactive training by Paul Ekman (www.paulekman.com/product/pictures-of-facial-affect-pofa/) and were equalized for luminance and degraded by means of image pixel phase randomization with addition of Gaussian noise to produce three different noise levels: 0%, 40%, and 55% for both sets of images. Behavioral experiments were conducted outside the scanner to gain some rough estimates of error trials. Before the actual experiments, six subjects participated in the behavioral experiments outside the scanner designed to determine the highest difficulty (e.g., noise) levels with performance accuracy close to 70%. We first created three difficult conditions based on our initial guess and previous reports, asked subjects to perform 100 trials, and counted the error trials. Then, based on the results of error trials, we adaptively modified the conditions and repeated the same procedure until we determined the difficult level that provided behavioral accuracy close to 70%.

The visual stimuli (faces and houses) subtended 4.34° by 6.08° visual angles (see, Lamichhane et al., 2016).

Experiment 2: happy–angry face discrimination task. In the happy–angry face discrimination task, two sets of human face images, a happy set and an angry set, were used as stimuli. Each set consisted of eight images (four males and four females), which were degraded and subject to additional noise to make two stimulus categories: clear image category (0% noise) and a noisy image category (40% noise), which formed the variables of interest. The two noise levels were decided to make the task difficult at or above 70% behavioral accuracy, with similar piloting procedures mentioned earlier in the face–house experiment. Thus, fMRI analysis was carried out based on noise level, rather than the happy or angry face categories investigated in a previous study (Bajaj et al., 2013).

Experiment 3: audio-visual asynchrony and synchrony perception task. In the audio-visual discrimination task, we used pairing of a single auditory stimulus, a 440-Hz–30-ms tone, and a visual stimulus, a 30-ms yellow-red disc flash (0.7 cm radius). Here, the flash of light (visual stimuli) was presented at the central position on the computer screen and the beep sound (auditory stimuli) was delivered through a pair of earphones, one on each ear. The actual behavioral run outside the scanner was conducted after we identified the point of subjective simultaneity, that is, how far apart in time the asynchronously presented audio and visual pair could be perceived as synchronous (for detail, see (Lamichhane et al., 2015b)). For this purpose, we presented audio and visual stimuli with a systematically varying asynchrony lag of 66.6, 83.3, 100, 116.6, 133.3, 150, and 166.6 ms, 20 trials for each lag totaling 140 trials. The choice of these lags was based on the previous studies at which humans can detect audiovisual asynchrony (Pons et al., 2014; van Eijk et al., 2008; van Wassenhove et al., 2007; Zampini et al., 2005; Zampini et al., 2003). The inter-trial interval (the pause, τ, based on the previous studies) was chosen randomly between 1000–1160 ms. We looked at the fraction of the trials from this run and chose the time lag (ΔT), as a threshold value, in which performance accuracy was 50:50 or close to it for the trials that were perceived as synchronous or asynchronous. For the recordings outside and inside the scanner, the time lags (ΔT) were varied beyond the individual's threshold value for audio-visual simultaneity with an increment between -16.6 ms and +16.6 ms and, for an fMRI session, τ was 1666–1926 ms.

Experiment 4: RDM direction discrimination task. In the RDM direction discrimination task, randomly moving noisy field of dots were used as stimuli and were presented within a circular aperture at the center of screen. In RDM, the coherence level was determined by the percentage of dots moving in the left or right direction while the remaining dots were moving in the random direction. The dot motion was induced by redrawing dots at a neighboring spatial location after 50 ms within black background circular aperture of 7.5 cm diameter for 34 ms in which dot appeared to move between 3° and 7°/s and at a density of 16.7 dots per deg^2/s.

We manipulated task difficulty level by mixing red and green dots in our RDM. First, we varied the proportion of the dots that are either moving to the left or right independent of color. Second, out of two colors, we assigned the green color for the dots that are moving in particular direction (either to the left or right direction only) and red to the dots that were moving in a random direction. With this manipulation we introduced three coherence levels in RDM (12%, 20% and 100%) in both color coherence (C) and color incoherence (IC) conditions. For example, in 20% C, the 20% of dots were green and all moved in one direction (left or right) while the 80% of dots were red and moved in random directions. Similarly, in 20% IC, RDM still consisted of 20% of green and 80% red dots. However only 20% of dots independent of color were moving in a particular direction while the remaining 80% were moving in random directions. However, in 100% C and IC (50% red dots and 50% green dots), all moved in one direction, so we refer to this stimulus condition simply as 100% (for greater details, see (Lamichhane et al., 2016).

The stimuli features are displayed in (i) of A, B, and D in Figure 1 and details about trial sequence are shown in (ii) of A, B, D, and in C (Fig. 1) for these tasks.

Data acquisition and analysis

In all of our experiments, data were collected in two separate sessions: the first session involved acquiring behavioral data (behavioral performance and RT) outside the MRI scanner and the second session was inside the scanner where we acquired both fMRI data and behavioral performance. Subjects indicated their decisions by keyboard presses outside the scanner and button presses on a response box inside the MRI scanner. Outside the MRI scanner, participants were seated about 70 cm away from the computer screen used to present the stimuli and indicated their decisions as quickly and as accurately as possible by left/right mouse clicks and pressed the space bar in the computer keyboard to proceed to the next trial. Inside the MRI scanner, they were required to focus on the central crossbar, perceived the presented stimuli, waited for the display of a question mark on the screen, and then indicated their choice by pressing the left/right key on a button box with either their right index or middle finger. This was to avoid recruiting brain motor response along with the PDM-related brain areas. Thus, we recorded RT only outside the scanner. The stimulus software presentation (www.neurobs.com) was used to display stimuli and to randomize task trial sequences.

In the face–house discrimination task, participants were asked to indicate their decisions by the right mouse click if they decided that the presented picture was house and left mouse click for face picture outside the scanner, and inside the scanner the correct responses for houses and faces were right button and left button clicks, respectively. Similarly, the correct response for happy faces was left mouse and left button and that of angry faces was right mouse and right button press outside and inside the scanner, respectively. In audiovisual task, participants reported their perception by left mouse and left button if they perceived synchrony or right mouse and right button for asynchrony. Similarly, in RDM, the left mouse and left button clicks were for leftward moving dots and the right mouse and right button were for rightward moving dots.

Outside the fMRI scanner. In face–house discrimination task, the behavioral study consisted of a single run. There were three noise-level conditions and each condition was repeated 60 times (30 times each for faces and houses) in a random order, generating 180 trials in total. In happy–angry face discrimination task, we have one functional run where each condition (clear and noisy condition) was presented 60 times (30 times each for happy faces and for angry faces) in a random order, totaling 120 trials. In audiovisual asynchrony and synchrony perception task, the pair of stimuli was presented 60 times, 20 at each ΔT. In RDM direction discrimination task, RDM stimuli with identical parameters (12% and 20% C, 12% and 20% IC, 100%) were presented for 1 sec as a single event and consisted of a single run. Each condition was presented 30 times, totaling 180 trials. Both behavioral performance and RT were recorded outside the scanner.

Inside the fMRI scanner. Inside the fMRI scanner, fMRI data were acquired and behavioral responses were recorded.

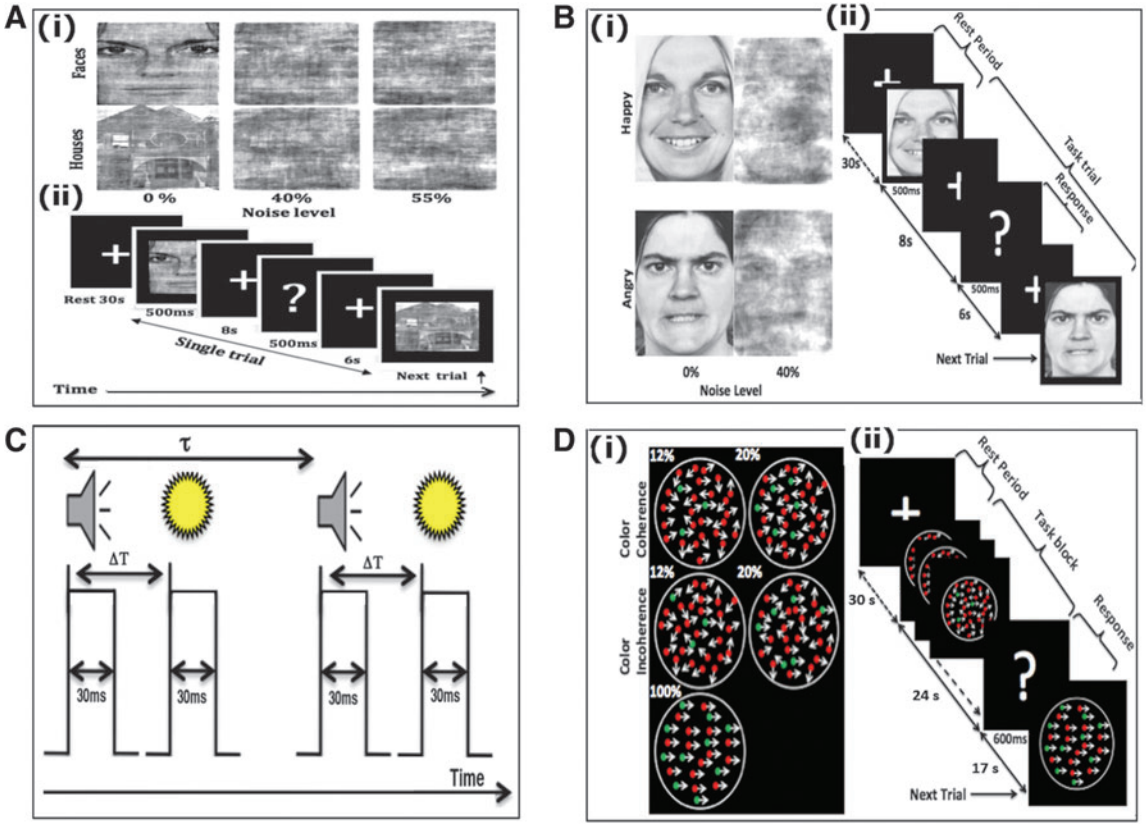

FIG. 1. Experimental paradigms. **(A)** Face–house discrimination task: **(i)** sample images at three noise levels for face and house stimuli set. **(ii)** task paradigm during a functional run, starting from the initial 30-sec rest followed by a task trial that included 500 msec stimulus presentation, 8 sec of decision time, and 500 msec display of a question mark, requiring participants to indicate their decision within the next 6 sec (Lamichhane and Dhamala, 2015a). **(B)** Happy–angry face discrimination task: **(i)** sample images at two noise levels of both happy and angry stimuli set. **(ii)** task paradigm during the functional experiment starting from initial 30-sec rest followed by task trial with a brief stimulus presentation for 500 msec duration, 8 sec of decision time, followed by a briefly presented question mark for 500 msec referring subjects to indicate their decision within the next 6 sec (Bajaj et al., 2013). **(C)** Audiovisual asynchrony and synchrony perception task: task paradigm during the functional experiment started with initial 30 sec of rest followed by task blocks and 35 sec of rest at the end of the run. There were two types of block: multisensory blocks (beep–flash pairs were presented for 30 msec, as shown in figure) and unisensory blocks (flash only or beep only were presented, not shown in figure). The time intervals between a flash and a beep sound (ΔT) varied from participant to participant. Stimuli within the block were presented with the random pause (τ) of 1666 to 1926 msec followed by the cue of 600 msec at the end of each block, totaling about 24 sec of one block. Participants were asked to respond after the cue was presented. In unisensory blocks, no question was asked about asynchrony and synchrony perception at the end of block (see Lamichhane and Dhamala, 2015b). **(D)** RDM direction discrimination task: **(i)** schematic representation of RDM stimuli: color coherence 12% and 20% (top), color incoherence 12% and 20% (middle) and 100% (bottom). **(ii)** Task paradigm during the functional experiment started with initial 30-sec rest followed by the block of RDM presented for 15 consecutive times for the total of 24 sec. A question mark presented for 600 msec asking subjects to indicate their decision, which is followed by 17 sec of pause. RDM, random dot motion. (for detail, see Lamichhane et al., 2016). Color images available online at www.liebertpub.com/brain

Each functional session started with 30 sec of initial rest and ended with 35 sec of final rest. Participants performed face–house categorization tasks in three functional runs, each 614 sec long, the number of trials for each noise-level condition was 36 (18 faces and 18 houses), and there were a total of 108 for all three conditions in each run. Stimuli were presented in a random order as in an event-related design within each run. In happy–angry face discrimination task, subjects performed two functional runs; each of 674 sec long and the total number of trials was 80, that is, 40 trials for each condition (clear and noisy).

In audiovisual asynchrony and synchrony perception task, data were recorded in a single functional run, there were 24 multisensory (both a flash of light and a beep sound) task blocks and 8 unisensory (either a flash of light or a beep sound) task blocks, and within a block, given stimuli were presented eight times. Similarly, in RDM direction discrimination tasks, there were 12 trials for each condition (RDM with identical parameters either 12%, 20% C or 12%, 20% IC and 100% presented for 15 consecutive times, for the total of 24 sec, in a block), all together 72 trials inside the scanner in two sessions. In this task, we did not find any statistical significant difference on behavioral response and RT between 12% and 20% C and IC stimulus conditions. We then combined the data and used three stimulus conditions: 12% and 20% C, 12% and 20% IC, and 100% for further analysis. The experimental details of these four tasks are provided in Table 1.

Table 1. Summary: Experimental Details on Four Tasks

		Outside the scanner	*Inside the scanner*
Face–house task	$n = 33$ (17 F, 16 M) m = 27.5 ± 4.7 years	No. of run = 1 No. of noise level = 3 No. of trials per noise level = 60	No. of run = 3 No. of noise level = 3 No. of trials each noise level = 36 Scanning time = 614 sec/run
Happy–angry task	$n = 32$ (16 F, 16 M) m = 27.6 ± 4.7 years	No. of run = 1 No. of noise level = 2 No. of trials per noise level = 60	No. of run = 2 No. of noise level = 2 No. of trials each noise level = 40 Scanning time = 674 sec/run
Audiovisual task	$n = 33$ (17 F, 16 M) m = 27.5 ± 4.7 years	No. of run = 2 Run 1 No. of time lags for SOA = 7 No. of trials per lag = 20 Run 2 No. of time lags for SOA = 3 No. of trials per lag = 20	No. of run = 1 No. of multisensory blocks = 24 No. of unisensory blocks = 8 Scanning time = 898 sec/run
Random dot motion task	$n = 32$ (16 F, 16 M) m = 27.6 ± 4.7 years	No. of run = 1 No. of conditions = 2 (coherence, incoherence) No. of coherence/incoherence level = 3 No. of trials per condition for each level = 30	No. of run = 2 No. of conditions = 2 (coherence, incoherence) No. of coherence incoherence level = 3 No. of trials per condition for each level = 12 Scanning time = 810 sec/run

n, number of participants; m, mean age; F, female; M, male; SOA, stimulus onset asynchrony; ±values, standard deviations.

Participants' behavioral performance, both outside and inside the scanner, was analyzed by using MATLAB. Trial by trial RTs of each participant from outside scanner button presses were separated and averaged across noise level in each task condition. No RT calculation was done for the recorded behavioral data inside the scanner. Paired *t*-tests were used to assess the significance levels of performance accuracy and RT across noise levels.

fMRI data

The whole-brain MRI was done on a 3-Tesla Siemens scanner available at the Georgia State University and Georgia Institute of Technology Center for Advanced Brain Imaging, Atlanta, Georgia. High-resolution anatomical images were acquired for anatomical references using a magnetization-prepared rapid gradient-echo sequence (with repetition time [TR] = 2250 msec, echo time [TE] = 4.18 msec, flip angle = 9°, inversion time = 900 msec, voxel size = $1 \times 1 \times 1\ mm^3$). The functional scans were acquired with T2*-weighted gradient echo-planar imaging protocol with the following parameters: TE = 30 msec, TR = 2000 msec, flip angle = 90°, voxel size = $3 \times 3 \times 3\ mm^3$, field of view = 204×204 mm, matrix size = 68×68 and 37 axial slices each of 3 mm thickness. MRI data were analyzed using Statistical Parametric Mapping (SPM8; Wellcome Trust Center, London, www.fil.ion.ucl.ac.uk/spm), which included slice timing correction, motion correction, coregistration to individual anatomical image, and normalization to Montreal Neurological Institute (MNI) template (Friston et al., 1995). Spatial smoothing of the normalized image was done with an 8-mm isotropic Gaussian kernel. A random-effect, model-based, univariate statistical analysis was performed in a two-level procedure. In all four experiments, we used the parameterization above and the same MRI data analysis procedures, unless otherwise stated.

At the first level, a separate general linear model (GLM) was specified according to the task sequences and behavioral responses for each participant. Only correct trials for each condition (noise levels: 0%, 40%, 55% in face–house discrimination task; 0%, 40% in happy–angry face discrimination task; asynchrony and synchrony conditions in audiovisual asynchrony and synchrony perception task; 12% and 20% C and IC, and the 100% condition in RDM direction discrimination task), rest and six motion parameters were included in GLM analysis. We restricted our analysis to correct trials because there were very few incorrect trials, especially in easy task conditions, which were not enough for reliable estimates of differences across conditions. The six motion parameters were entered as nuisance covariates and were regressed out of the data. Individual contrast images of all participants resulting from the first-level analysis were then entered into a second-level analysis for a separate one-sample *t*-test. The resulting summary statistical maps were then thresholded and overlaid on high-resolution structural images in MNI orientation. The activation clusters were identified under the statistical significance $p < 0.05$, familywise error (FWE) correction, for multiple comparisons correction, and cluster extent $k \geq 10$; except in moving dot task where statistical significance was $p < 0.01$, FWE correction.

Connectivity analysis

The regions of interest (ROIs) were based on activation t-maps. We defined three ROIs, by generating a sphere of 6 mm radius in MarsBar (Brett et al., 2002), for the SN nodes. The center coordinates were (−6, 11, 52) for the dACC, (−30, 20, 4) for the left insula (lAI), and (33, 20,

4) for the right insula (rAI) in all tasks. These coordinates matched exactly or were very close to local maxima from the second-level group analysis of fMRI data (Table 2). The time courses from all the voxels within each ROI and all subjects were extracted for each experimental task for the aforementioned conditions. We performed Granger causality (GC) analysis to characterize the directional influences between ROIs.

Since fMRI-BOLD signals are believed to originate from smoothing of neuronal activity by the hemodynamic response function (Aguirre et al., 1998; Handwerker et al., 2004), we constructed hidden neural signals by hemodynamic deconvolution for each ROI data, as suggested in previous studies (David et al., 2008; Handwerker et al., 2004; Roebroeck et al., 2011; Valdes-Sosa et al., 2011; Wu et al., 2013). We used these deconvolved fMRI-BOLD time series for functional directed connectivity calculation. The ensemble mean removed segmented deconvolved time series from separate voxels and subjects were treated as trials for reliable estimates of the network measures. We calculated the frequency-dependent parametric GC spectra (Dhamala et al., 2008) for pairs of ROIs. GC spectra can be estimated by parametric and nonparametric methods (Dhamala et al., 2008). GC spectra from the parametric and nonparametric match very well when many data samples are collected (long time series and many trials) and appropriately modeled in the parametric approach. Theoretically, time series need to be modeled by infinite series of autoregressive processes. In practice, we have finite data points, but we still need to find an appropriate model order for a given data. As it is often difficult to find an appropriate model order for brain data with the traditional Akaike information criterion and Bayesian information criterion (Antzoulatos and Miller, 2014; Dhamala et al., 2008), when appropriately modeled, the parametric method yields GC values that have less bias for short time series data (please see the appendix of Dhamala et al., NeuroImage, 2008). To take advantage of both approaches, in this study, we determined the optimal model order for the parametric method using a method developed recently (Adhikari et al., 2014) by comparing the power spectra from nonparametric and parametric approaches at different model orders, and choosing the model order yielding the lowest power difference. From the parametric spectral GC, the time domain values were obtained by integrating the causality spectra

Table 2. The Brain Activations for Various Contrasts

Contrast	*Brain regions*	*Cluster size*	*Voxel t (z-equivalent)*	*MNI coordinates x, y, z*
Noisy (faces+houses)	R Insula	54	8.75 (6.21)	33, 20, 4
vs. clear (faces+houses)	dACC	109	7.96 (5.87)	−6, 17, 52
	L Insula	40	7.85 (5.82)	−30, 23, 1
	L IFG	25	6.70 (5.26)	−39, 5, 34
	R IFG	27	6.67 (5.24)	45, 8, 25
Noisy vs. clear	R Insula	64	8.94 (6.24)	33, 20, 4
(happy+angry faces)	L Insula	65	8.12 (5.90)	−30, 23, 4
	dACC	34	5.93 (4.93)	0, 17, 52
Audiovisual vs. (beep+flash)	dACC	122	9.78 (6.61)	−6, 11, 52
	R MOG	71	8.84 (6.24)	27, −97, −5
	L IFG	47	8.42 (6.07)	−60, 8, 28
	R Thalamus	101	8.41 (6.07)	3, −3, 1
	L Insula	84	7.76 (5.78)	−30, 20, 4
	R Insula	117	7.62 (5.73)	33, 20, 4
	L MOG	37	6.80 (5.31)	−27, −94, −5
	L IPL	42	6.67 (5.24)	−33, −49, 46
Moving dots (12%+20%)	R VC	1026	13.17 (7.59)	24, −88, −11
C+(12%+20%) IC	L VC	774	12.66 (7.46)	−21, −97, 7
vs. 100% (C+IC)	R MT	103	9.86 (6.59)	48, −67, 4
	R Insula	108	9.71 (6.53)	30, 20, 4
	L Insula	50	7.81 (5.76)	−30, 20, 4
	R dlPFC	356	8.74 (6.16)	42, 11, 22
	R SEF	146	8.42 (6.03)	36, −1, 49
	L IPL	75	7.92 (5.81)	−30, −49, 46
	R IPL	144	7.69 (5.71)	39, −40, 43
	L MT	28	7.60 (5.66)	−42, −64, 4
	dACC	14	7.58 (5.66)	−6, 11, 52
	L dlPFC	59	7.35 (5.55)	−51, 2, 34
	R MOG	11	6.87 (5.31)	30, −67, 25
	L SEF	12	6.69 (5.22)	−33, −7, 52

The table above lists brain activations for various contrasts. It includes the information about the anatomical locations, cluster sizes, *t*-value (z-score), and MNI coordinates for the activations under statistical significance $p < 0.05$ familywise error correction, for multiple comparisons correction, and cluster extent $k \geq 10$.

C, color coherence; IC, color incoherence; L, left; R, right; dACC, dorsal anterior cingulate cortex; dlPFC, dorsolateral prefrontal cortex; IFG, inferior frontal gyrus; IPL, inferior parietal lobule; MFG, middle frontal gyrus; MNI, Montreal Neurological Institute; MOG, middle occipital gyrus; MT, middle temporal cortex; SEF, supplementary eye fields; VC, visual cortex (occipital lobe).

over the entire frequency range. The significant GC spectra, and hence the significant network connections, were defined by setting a GC threshold above the random noise baseline. To compute the threshold value of GC, we constructed a set of surrogates by randomly permuting trial data from each subject and used a random permutation technique (Blair and Karniski, 1993; Brovelli et al., 2004). The threshold was thus based on the null hypothesis that there was no statistical interdependence between nodes when trials were randomized. We computed GC spectra from all possible pairs of ROIs with a minimum of 1000 random permutations and picked maximum GC on each permutation. By fitting the distribution with a gamma distribution function (Dhamala et al., 2008), we obtained the threshold for GC spectra at significance $p < 10^{-3}$ from the ROIs from each experiment separately. This threshold GC was used to identify significantly active directed network activity among three ROIs calculated in pairwise GC analysis. We have also performed the conditional GC analysis and ruled out the interactions that were found mediated by another node, if any. We computed the time domain GC values for significantly active network directions and performed paired *t*-tests on these values to find the significant network modulation in our tasks by different noise levels in the task stimuli.

Results

Behavioral response

In the face–house discrimination task, the mean performance accuracy rate decreased with noise outside of the scanner 99.3% ± 1.3% (0% noise), 89.5% ± 7.3% (40% noise), and further to 68.5% ± 7.9% (55% noise). Values ± represent the standard deviations throughout the article. Similar decreases occurred inside the scanner (97.9% ± 3.4%, 87.0% ± 7.9%, and 65.1% ± 9.8%). Accuracy decreased significantly with noise level ($p < 0.001$; Fig. 2A). RTs

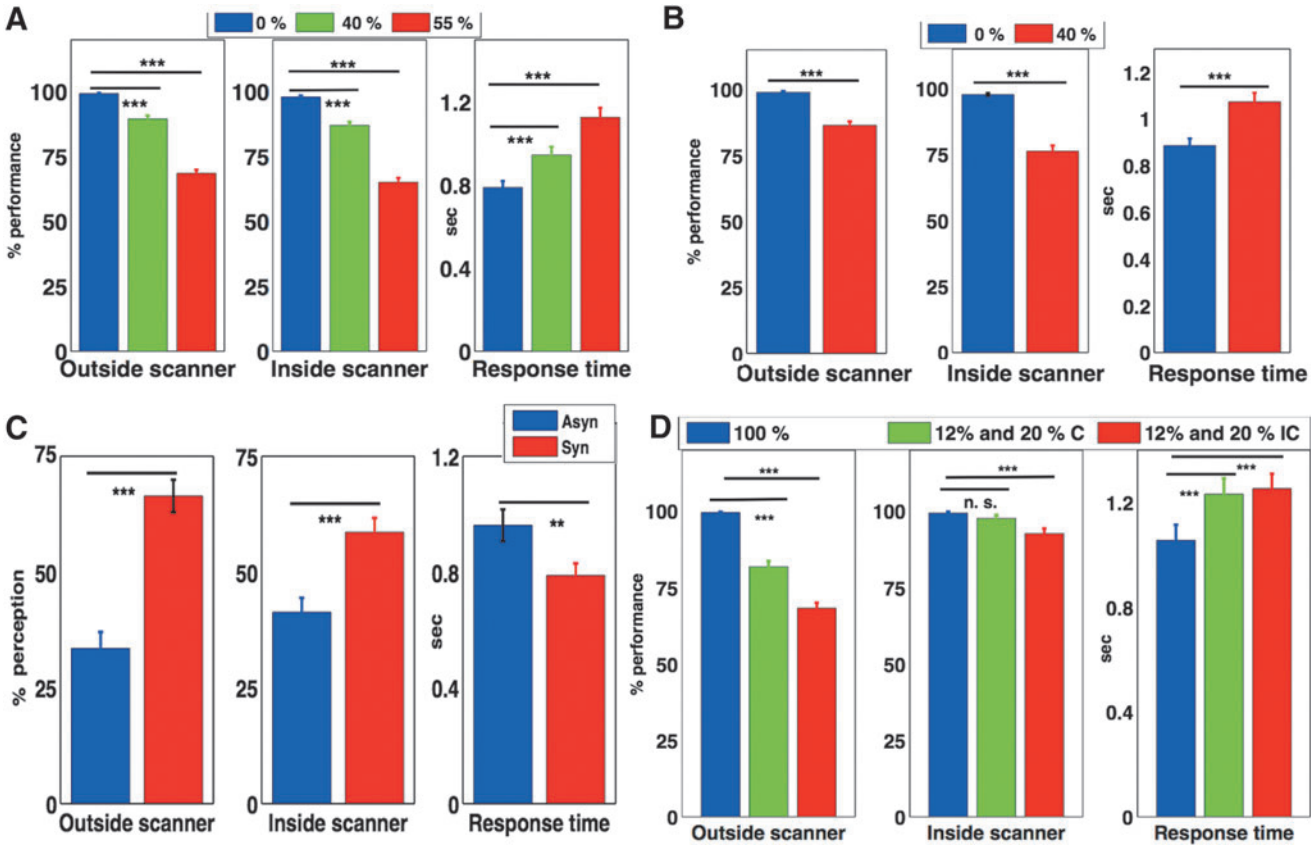

FIG. 2. Behavioral results. **(A)** Face–house discrimination task: the mean performance (%) is significantly decreased ($p < 0.001$) with increase in noise levels (0% noise level to 40% noise level and then to 55% noise level) both outside (first column) and inside (second column) the fMRI scanner and the RT outside the fMRI scanner (third column) is significantly increased ($p < 0.001$) with the increase in noise levels. **(B)** Face–house discrimination task: mean performance (%) is significantly decreased ($p < 0.001$) and RT is significantly increased ($p < 0.001$) when noise level is increased from 0% to 40%. **(C)** Audiovisual asynchrony and synchrony perception task: behavioral responses were categorized based on participants' perception of asynchrony and synchrony. The plots show mean asynchrony perception (Asyn) and synchrony perception (Syn) in percentage outside (first column), inside (second column) the fMRI scanner, and RT outside the fMRI scanner (third column), which are statistically different ($p < 0.01$). **(D)** RDM direction discrimination task: the bar plots represent mean performance (%) outside (first column), inside (second column) the fMRI scanner, and RT outside the fMRI scanner (third column) for three task levels (100%, 12%, and 20% coherence, and 12% and 20% incoherence, respectively). Error bars represent standard error of the mean. $^{**}p < 0.01$ and $^{***}p < 0.001$. fMRI, functional magnetic resonance imaging. n. s., not significant; RT, response time. Color images available online at www.liebertpub.com/brain

significantly increased with noise level ($p < 0.001$). The mean RTs were 0.79 ± 0.17 sec (0% noise), 0.94 ± 0.22 sec (40% noise), and 1.13 ± 0.28 sec (55% noise; Fig. 2A).

In the happy–angry face discrimination task, participants correctly responded with an average rate of $98.9\% \pm 2.2\%$ for clear images, with $86.4\% \pm 8.3\%$ for noisy images outside the scanner, and $97.7\% \pm 3.2\%$ and $76.3\% \pm 11.9\%$, respectively, inside the scanner (Fig. 2B). More time was taken to respond to noisy images (1.07 ± 0.21 sec) compared to clear images (0.88 ± 0.17 sec). Behavioral accuracy decreased significantly with noise both inside and outside the scanner ($p < 0.001$). The addition of noise on images significantly increased RT ($p < 0.001$; Fig. 2B) in addition to significantly decreasing the performance accuracy.

In the audiovisual asynchrony and synchrony perception task, we categorized the behavioral responses based on participants' perception of asynchrony and synchrony. The mean performance rate outside the scanner was about 34% and 66% (±19.7%) for asynchrony and synchrony perception, respectively. Similarly, the mean performance rate inside the scanner was 41% and 61% (±17.6%). Discrimination among these percepts differs statistically both outside and inside the scanner ($ps < 0.001$). More time was taken to respond with the asynchrony perception (0.96 ± 0.30 sec) compared to synchrony perception (0.79 ± 0.20 sec; $p < 0.01$). These results are shown in Figure 2C.

In RDM direction discrimination task, participants' performance accuracy rates for correctly deciding the direction of randomly moving dots were $99.6\% \pm 1.4\%$ for 100%, $81.8\% \pm 10.3\%$ for combined 12%, 20% C, and $68.3\% \pm 9.7\%$ for combined 12%, 20% IC outside the scanner. Inside the scanner, accuracies were $99.4\% \pm 2.4\%$, $97.7\% \pm 6.3\%$, and $92.7\% \pm 9.4\%$, respectively. Compared to 100%, combined 12%, 20% C and combined 12%, 20% IC conditions had significantly lower accuracies ($p < 0.001$) in the recordings outside the scanner, while inside the scanner, performance accuracy was significantly reduced ($p < 0.001$) in case of combined 12%, 20% IC in comparison with 100%. Furthermore, RT for the participants' to report their decision increased from 1.07 ± 0.33 sec (100% condition) to 1.23 ± 0.33 sec (C) and 1.25 ± 0.31 sec (IC). Behavioral accuracy was significantly greater ($p < 0.001$) and RT significantly lower ($p < 0.001$) for IC, C compared to 100% condition outside the scanner as shown in Figure 2D.

Brain response

In the face–house discrimination task, brain activations were computed by contrasting the difficult pictures (40% and 55% noise level combined and independent of faces and houses) versus clear pictures (0% noise level). We found significant brain activations in prefrontal cortices, left and right AI, dACC, listed in Table 2.

In happy–angry face discrimination task, bilateral AIs and dACC were found activated more by 40% noisy pictures compared to clear (0% noise) pictures, as shown in Table 2.

In audiovisual asynchrony and synchrony perception task, we contrasted asynchrony perception+synchrony perception to auditory (only beep)+visual (only flash). The significant brain activations were found in the dACC, AIs, bilateral middle occipital gyrus, inferior frontal gyrus, thalamus, and inferior parietal lobule, as shown in Table 2. In this study, we used GC techniques to study directed functional connectivity patterns within main SN nodes at the two-perception level (asynchrony and synchrony perception). One set of data was analyzed in a previous study (Lamichhane and Dhamala, 2015b) that used a different effective approach: dynamic causal modeling (DCM) to explore the effective connectivity

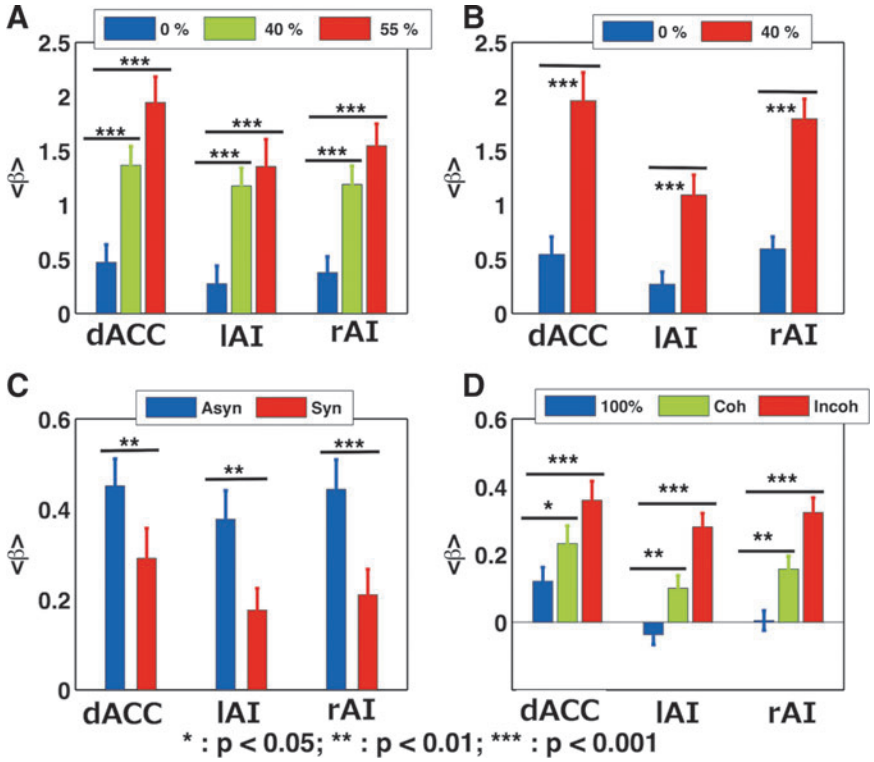

FIG. 3. Mean contrast values: Contrast values (β) were calculated, for noise levels: 0%, 40%, and 55% face and house stimuli **(A)**; 0% and 40% happy and angry face stimuli **(B)**; for asynchrony perception and synchrony perception for audiovisual (a beep sound and a flash of light) stimuli **(C)**; and for 100%, 12%, and 20% coherently and 12% and 20% incoherently moving dots **(D)**, from dACC, left insula (lAI), and right insula (rAI) from each subject and used to calculate mean beta and the standard error of the mean. AIs, anterior insulae; dACC, dorsal anterior cingulate cortex. Color images available online at www.liebertpub.com/brain

in audiovisual perceptual task regardless of difficulty levels. In this work, we regarded detecting asynchrony and synchrony as two-task difficulty levels. This is based on previous studies (Adhikari et al., 2013; Dhamala et al., 2007; Lamichhane and Dhamala, 2015b; Stevenson and Wallace, 2013; Vatakis and Spence, 2006) that people find it more difficult to detect asynchrony compared to synchrony in audiovisual events.

In the RDM direction discrimination task, we have contrasted brain activity for 12% and 20% stimulus conditions (both C and IC) with that of the 100% condition. We found significant activation for bilateral visual cortex, middle temporal, insulae (AIs), frontal (dorsolateral prefrontal cortex, supplementary eye fields) and parietal (inferior parietal lobule) cortices and dACC, as shown in Table 2. All the activations shown in Table 2 were statistically significant for FWE correction, $p < 0.05$ and cluster-level threshold, $k > 10$; except in moving dot task where statistical significance was $p < 0.01$ (FWE). The coronal slice in Figure 4 shows activation in bilateral AIs and dACC.

BOLD response (contrast values)

We carried out the analysis to answer how node activity within the SN gets modulated with task difficulty (or with noise level for different stimulus conditions). We calculated region-specific beta values (β) from each participant for each stimulus condition for all the noise levels considered, in these tasks, and were averaged to produce average β from dACC, left insula (lAI) and right insula (rAI). The node activity, indicated by contrast values, was significantly modulated ($p < 0.05$) due to task difficulty, as shown in Figure 3A for the face–house discrimination task for three noise levels: 0%, 40%, and 55%; Figure 3B for happy–angry face discrimination task for 0% and 40% noise levels; Figure 3C for asynchrony perception and synchrony perception for audiovisual asynchrony and synchrony perception task, and Figure 3D for the RDM direction discrimination task for 100%, combined 12%, 20% coherently and combined 12%, 20% incoherently moving dots.

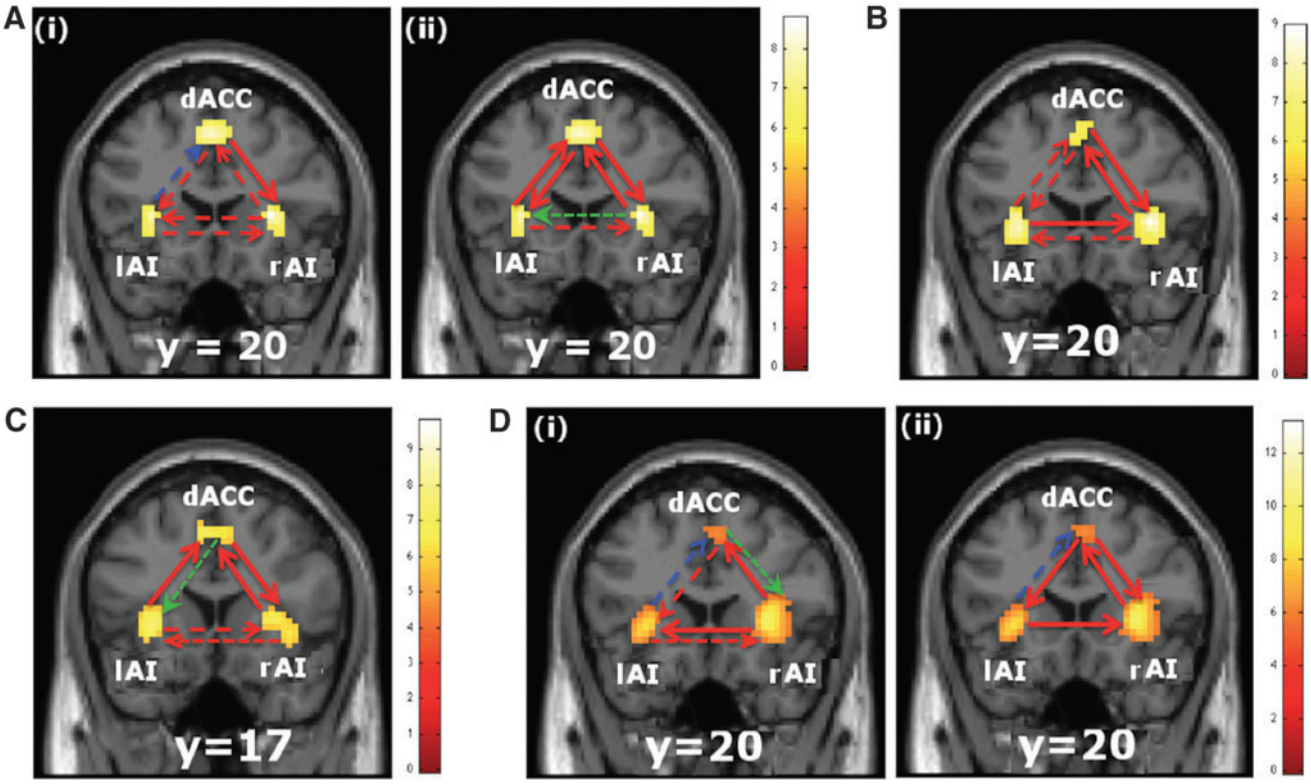

FIG. 4. Salience network interactions: Significant causal interaction directions among three nodes, dACC, left insula (lAI), and right insula (rAI), during four perceptual tasks are shown. The significant causal connections as determined by using permutation threshold criteria and by ruling out the mediated interactions (as shown by green dotted line with an arrowhead) using conditional Granger causality analysis are shown either by a solid line with an arrowhead or dotted line with an arrowhead. Red solid line with an arrowhead represents an increase in causal interactions ($p < 0.05$), whereas the dotted line (red or blue) with an arrowhead represents insignificant change in interactions when the causal strengths between conditions were compared. Here, red/blue dotted lines represent the increased/decreased causal interactions. **(A)** Network interactions during face–house discrimination task when connection strengths during **(i)** 40% noisy face–house stimuli, and **(ii)** 55% noisy face–house stimuli were compared to 0% noisy face–house stimuli, respectively. **(B)** Network interactions during happy–angry face discrimination task when causal influences for 40% noisy happy–angry face stimuli were compared to 0% noisy happy–angry face stimuli. **(C)** Network interactions during audiovisual asynchrony and synchrony perception task where the causal influences in asynchrony were compared to synchrony. **(D)** Network interactions during RDM direction discrimination task when connection strengths during **(i)** 12% and 20% color coherence, and **(ii)** 12% and 20% color incoherence were compared to 100% dots moving in a particular direction, respectively. For better comparisons of the results, we have used the coronal slice view showing three nodes, which may not necessarily show their peak activation voxel locations. Color images available online at www.liebertpub.com/brain

SN activity

We computed GC spectra to assess oscillatory network interactions among the three nodes: dACC, lAI, and rAI that form the SN. GC (pairwise GC) spectra were calculated separately for different noise levels for each condition in all four tasks. At first, we used the permutation threshold criteria to find the significant causal interaction directions and then, the conditional GC to rule out the mediated interactions (details in Materials and Methods section). The significant causal connections among these three nodes are shown in Figure 4 by either a solid line or a dotted line (red or blue) with an arrowhead. The green dotted lines represent the directions of mediated interactions and are ruled out. For example, in Figure 4B, all the interaction directions are significant for clear (0% noise) and noisy (40% noise) happy–angry face images. Regarding solid lines, they represent the significant change in causal interactions when compared between conditions (noisy (40% noise) case when compared with clear (0% noise) case), as shown in Figure 4B. Green dotted line with an arrowhead (e.g., in Fig. 4C) represents the direction ruled out in asynchrony and synchrony perception conditions in audiovisual task. The node pointed to by the arrowhead receives the causal influence from the node the line starts from.

Our interest was to find out how the causal interactions changed due to increased noise level in stimuli, which increased the task difficulty level. The time domain GC values calculated from the entire frequency range from all the subjects were compared across conditions for statistical significance using paired *t*-tests. Red solid lines with an arrowhead represent a significant ($p < 0.05$) increase in directed interactions. However, the dotted lines with an arrowhead are used to indicate that the results are insignificant, red dotted lines are for increase, and blue dotted lines are for decrease in GC, as shown in Figure 4. How GC values changed when the comparison was made between 40% noise-level and 0% noise-level face–house stimuli are shown in Figure 4A (i). The significant increase in causal influence was found to occur for the dACC to rAI. The bidirectional interactions between lAI and rAI, and lAI and dACC did not change significantly. The bidirectional causal interactions between dACC and lAI, and dACC and rAI increased significantly [Fig. 4A (ii)] when we compared the causal interactions for 55% noise level with 0% noise level in face–house stimuli. The causal influences that rAI received from lAI and dACC significantly increased when the causal interactions for 40% noisy happy–angry faces were compared with that of 0% noisy happy–angry faces, as shown in Figure 4B. Also, there was significant increase in causal interaction from rAI to dACC for 40% noisy versus 0% noisy happy–angry face stimuli, but interactions of lAI from and to dACC did not increase significantly (Fig. 4B). In the audiovisual asynchrony and synchrony perception task, when we compared asynchrony perception with synchrony perception, we found the causal influences from lAI and rAI to dACC, and from dACC to rAI increased significantly, but not from lAI to rAI and vice-versa (Fig. 4C). When we compared the causal influences between combined 12% and 20% C with 100%, in case of RDM direction discrimination task, significant increases in causal interactions were found from rAI to both dACC and lAI, whereas the interactions between lAI and dACC did not change significantly [Fig. 4D (i)]. When the comparison was done for combined 12% and 20% IC with 100%, we found significantly increased causal influences from lAI to rAI, rAI to dACC, dACC to lAI, and dACC to rAI, as shown in Figure 4D (ii). The causal influence decreased, but not significantly, from lAI to dACC in both of these comparisons [Fig. 4D (i), (ii)].

Across all these tasks, there was a bidirectional network activity between rAI and dACC. This network activity increased with task difficulty, as shown in Figure 4A (ii), B, C, D (ii). For difficult tasks, the causal interactions between dACC and lAI were bidirectional except for audiovisual discrimination task. The network activity between dACC and lAI was bidirectional for the face–house discrimination tasks [Fig. 4A (ii)], but unidirectional from lAI to dACC in audiovisual asynchrony and synchrony perception (Fig. 4C) and from dACC to lAI in RDM discrimination task for IC (12% and 20%), as in Figure 4D (ii) compared to easy tasks (clear, less ambiguous stimulus types). The increase in network activity from lAI to rAI was significant for noisy compared to clear happy–angry facial stimuli and IC (12% and 20%) compared to 100% [Fig. 4D (ii)], but the opposite relationship was found for C (12% and 20%) compared to 100% [Fig. 4D (i)].

In summary, when difficult decisions were compared with easy decisions, we found (1) significantly increased bidirectional causal influences between rAI and dACC in all tasks, (2) rAI received significantly higher causal influences from lAI in happy–angry face discrimination and RDM discrimination tasks, (3) dACC exerted significantly stronger causal influences to lAI in all tasks except audiovisual asynchrony and synchrony perception task, and (4) lAI exerted significantly greater causal influences to dACC in face–house discrimination task and audiovisual asynchrony and synchrony perception task.

Discussion

The functional role of the SN underlying PDM processes has not been sufficiently examined. We used four sensory discrimination tasks in visual and audiovisual domain with varying degree of degraded sensory input, measured fMRI-BOLD signal, and used spectral GC techniques to explore the role of SN in PDM. We found that the SN involved in all of the task conditions. The activity level as indicated by BOLD signal in SN nodes was found to increase with the increase in noise level or task difficulty. Our GC analysis showed that the key nodes in SN were functionally connected to each other and the directed functional connectivity strengths also increase with noise level. These task difficulty-dependent node and network activities within SN provide a strong support of the role of SN in PDM. Furthermore, these findings are consistent with the previously reported finding that the AIs and dACC serve as part of the decision-making network that integrates information and chooses one response over another (Lamichhane and Dhamala, 2015b) and supported by many other studies in the field (Ho et al., 2009; Krebs et al., 2012; Rushworth et al., 2004; Srinivasan et al., 2013; Venkatraman et al., 2009; Wiech et al., 2010; Woolgar et al., 2011).

Based on the results consistent with previous studies, we proposed that AIs, key nodes of SN, are involved in integrating information and processing (Gu et al., 2013; Lamichhane

and Dhamala, 2015b; Sterzer and Kleinschmidt, 2010). Although AIs were typically associated with social and affective tasks involving pain, empathy, disgust, and introspective processes (Craig, 2009; Singer et al., 2009), their role in information processing is also supported by their widespread efferent and afferent projections to and from the frontal, parietal, and temporal lobes (Mesulam and Mufson, 1982a, 1982b; Saper, 2002; van den Heuvel et al., 2009) and functional connection with a large-scale network of sensorimotor, affective, and cognitive control regions (Cauda et al., 2011; Chang et al., 2013; Deen et al., 2011; Touroutoglou et al., 2012). The significantly higher brain activity in AIs during the difficult task (stimuli with higher noise level or more ambiguity on stimulus features) conditions might reflect relatively greater task difficulty and indicate the need of more effort for the integration of information (Calvert, 2001; Tregellas et al., 2006) and PDM (Kosillo and Smith, 2010).

Neuroimaging studies provided the evidence that AIs and dACC have a close functional relationship in a wide range of tasks (Binder et al., 2004; Bushara et al., 2001; Dosenbach et al., 2007; Ham et al., 2013; Ho et al., 2009; Krebs et al., 2012; Lewis et al., 2000; Ploran et al., 2007; Tregellas et al., 2006; Venkatraman et al., 2009; Woolgar et al., 2011). Recent studies using DCM analysis have been shown that the input to insula (specially rAI) was higher compared to dACC (Ham et al., 2013; Lamichhane and Dhamala, 2015b). Our previous work (Lamichhane and Dhamala, 2015b) focused on correct trials only, but Ham and his colleagues work focused on error trials (Ham et al., 2013). Similar to the finding of Ham and colleagues, Cai and colleagues reported a greater rAI activity in ''unsuccessful stop'' trials than in ''successful stop'' trials and such rAI activity was found sensitive to the outcome of stopping but they found no support for AI role in error processing. The higher SN activity in error trials was interpreted as an effortful, but unsuccessful, force of the SN (Cai et al., 2014; Ghahremani et al., 2015). Hence it is possible that AI involved in processing information salience or relevance to a current task or goal and activated whenever the sensory input poses a challenge by sensory uncertainty or ambiguity, the disambiguation of which requires enhanced effort (Sterzer and Kleinschmidt, 2010). In our study, AI was possibly involved in integrating the sensory information salient to driving task-relevant behavior.

Our interpretation of this finding is in accordance to previously proposed role of AI that it may integrate behaviorally relevant stimuli (Menon, 2015) and that is further used by dACC (Lamichhane and Dhamala, 2015b). With the insular input, the dACC might be coordinating in selection of motor action and overcoming the conflict in decision-making (Botvinick et al., 2001, 2004; Botvinick, 2007; Ide et al., 2013). However, for a PDM task that does not require motor response, a detailed investigation of the coupling between AI and dACC is an interesting topic for future research.

In addition, the observed higher BOLD response in dACC during difficult compared to easier tasks might be due to the increased task demand of assessing information when the information is not straight forward (Nee et al., 2011; Rushworth et al., 2004; Taylor et al., 2007; Thielscher and Pessoa, 2007) and insufficient to support one action over another during goal-directed action selection (Dosenbach et al., 2007; Gluth et al., 2012; Holroyd and Yeung, 2012; Landmann et al., 2007; Medford and Critchley, 2010; Rushworth et al., 2007; Zysset et al., 2006). Although the dACC might access such information from widespread efferent and afferent projections to and from the large-scale network of sensory, affective, and cognitive regions (Cauda et al., 2011; Chang et al., 2013; Deen et al., 2011; Mesulam and Mufson, 1982a, 1982b; Saper, 2002; Touroutoglou et al., 2012; van den Heuvel et al., 2009), insular cortex influence might play an important role in the selection of appropriate choice in PDM in difficult task conditions. The observed load-dependent directed functional connections between dACC and AIs during tasks further support this notion as does a recent study where authors showed that intact white matter bundle projecting to/from dACC is important for performing tasks (Metzler-Baddeley et al., 2012). Lesions in this part of the brain can lead to difficulties in initiating complex voluntary movements and actions (Rushworth et al., 2004; Srinivasan et al., 2013; Williams et al., 2004). This conclusion is also supported by studies which state that the dACC is involved in guided action selection (Kennerley et al., 2006; Quilodran et al., 2008; Walton et al., 2004). Based on our evidence, we propose that dACC is responsible for high-level behavioral plans to achieve the goal of our moment-to-moment actions (Holroyd and Yeung, 2012).

The SN plays an important role in saliency detection, reactivity, facilitating access to attention and working memory resources once a salient event has been detected. Emerging evidence suggests that the SN plays a crucial role in switching between large-scale brain networks involved in externally oriented attention and internally oriented mental processes (Sridharan et al., 2008). During the performance of many cognitively demanding tasks, the SN shows increase in activation together with the lateral frontoparietal central executive network (CEN) whereas the default-mode network (DMN) shows decrease in activation below the resting baseline (Greicius et al., 2003; Raichle et al., 2001). Moreover, brain responses within these regions increase and decrease proportionately in relation to specific cognitive demands and task difficulty. Once a salient event is detected, the AI facilitates sustained processing by initiating appropriate transient control signals that engage cognitive and task control systems while suppressing the default-mode network (Sridharan et al., 2008). In this study, we have not examined into how important the SN is for the efficient regulation of activity in the default-mode network, efficient cognitive control, and better performance of cognitive control tasks. Furthermore, network activity exploring the information flow among these three networks, SN, CEN, and DMN, with task difficulty is left for future work, which will enhance our understanding about the brain mechanisms in PDM. A potential limitation of our study is that all tasks, although perceptual in nature, are different from each other in terms of stimulus modality and level of difficulties. The overall brain mechanisms (brain areas, including salience nodes and their network activities) might differ across these tasks. However, even though the tasks are different, the SN activity patterns and the network modulations uncovered here are quite similar for PDM difficulty.

In summary, the activity level based on BOLD signal changes in the SN nodes was found to increase with the task difficulty across four tasks. The network activity analysis showed that these nodes functionally interact with each

other and the network activity increases with task difficulty. These results provide a strong support for a functional role of the SN in PDM. These findings altogether provide new insights into the brain mechanisms and the general nature of high-level information processing, action selection, and perception to action mapping in goal-directed tasks.

Acknowledgments

We thank Crystal Smith and Eli Goshorn for writing computer programs for manipulating and controlling stimuli used in this study. This work was supported by an NFS CAREER award (BCS 0955037) to M. Dhamala.

Author Disclosure Statement

No competing financial interests exist.

References

Adhikari BM, Goshorn ES, Lamichhane B, Dhamala M. 2013. Temporal-order judgment of audiovisual events involves network activity between parietal and prefrontal cortices. Brain Connect 3:536–545.

Adhikari BM, Sathian K, Epstein CM, Lamichhane B, Dhamala M. 2014. Oscillatory activity in neocortical networks during tactile discrimination near the limit of spatial acuity. NeuroImage 91:300–310.

Aguirre GK, Zarahn E, D'Esposito M. 1998. The variability of human, BOLD hemodynamic responses. NeuroImage 8: 360–369.

Antzoulatos EG, Miller EK. 2014. Increases in functional connectivity between prefrontal cortex and striatum during category learning. Neuron 83:216–225.

Bajaj S, Lamichhane B, Adhikari BM, Dhamala M. 2013. Amygdala mediated connectivity in perceptual decision-making of emotional facial expressions. Brain Connect 3:386–397.

Binder JR, Liebenthal E, Possing ET, Medler AD, Ward BD. 2004. Neural correlates of sensory and decision processes in auditory object identiification. Nat Neurosci 7:295–300.

Blair RC, Karniski W. 1993. An alternative method for significance testing of waveform difference potentials. Psychophysiology 30:518–524.

Botvinick MM. 2007. Conflict monitoring and decision making: reconciling two perspectives on anterior cingulate function. Cogn Affect Behav Neurosci 7:356–366.

Botvinick MM, Braver TS, Barch DM, Carter CS, Cohen JD. 2001. Conflict monetoring and cognitive control. Psychol Rev 108:624–652.

Botvinick MM, Cohen JD, Carter CS. 2004. Conflict monitoring and anterior cingulate cortex: an update. Trends Cogn Sci 8:539–546.

Brett M, Anton J-L, Valabregue R, Poline J-B. 2002. Region of interest analysis using an SPM toolbox (abstract). Presented at the 8th International Conference on Functional mapping of Humal Brain, June 2–6, 2002, Sendai, Japan.

Brovelli A, Ding M, Ledberg A, Chen Y, Nakamura R, Bressler SL. 2004. Beta oscillations in a large-scale sensorimotor cortical network: directional influences revealed by Granger causality. Proc Natl Acad Sci U S A 101:9849–9854.

Bushara KO, Grafman J, Hallett M. 2001. Neural correlates of auditory-visaul stimulus onset asynchrony detection. J Neurosci 32:300–304.

Cai W, Ryali S, Chen T, Li CS, Menon V. 2014. Dissociable roles of right inferior frontal cortex and anterior insula in inhibitory control: evidence from intrinsic and task-related functional parcellation, connectivity, and response profile analyses across multiple datasets. J Neurosci 34:14652–14667.

Calvert GA. 2001. Crossmodal processing in the human brain: insights from functional neuroimaging studies. Cereb Cortex 1:1110–1123.

Cauda F, D'Agata F, Sacco K, Duca S, Geminiani G, Vercelli A. 2011. Functional connectivity of the insula in the resting brain. NeuroImage 55:8–23.

Chang LJ, Yarkoni T, Khaw MW, Sanfey AG. 2013. Decoding the role of the insula in human cognition: functional parcellation and large-scale reverse inference. Cereb Cortex 23:739–749.

Craig AD. 2009. How do you feel–now? The anterior insula and human awareness. Nat Rev Neurosci 10:59–70.

David O, Guillemain I, Saillet S, Reyt S, Deransart C, Segebarth C, Depaulis A. 2008. Identifying neural drivers with functional MRI: an electrophysiological validation. PLoS Biol 6:2683–2697.

Deen B, Pitskel NB, Pelphrey KA. 2011. Three systems of insular functional connectivity identified with cluster analysis. Cereb Cortex 21:1498–1506.

Dhamala M, Assisi CG, Jirsa VK, Steinberg FL, Kelso JA. 2007. Multisensory integration for timing engages different brain networks. NeuroImage 34:764–773.

Dhamala M, Rangarajan G, Ding M. 2008. Analyzing information flow in brain networks with nonparametric Granger causality. NeuroImage 41:354–362.

Dosenbach NU, Fair DA, Miezin FM, et al. 2007. Distinct brain networks for adaptive and stable task control in humans. Proc Natl Acad Sci U S A 104:799–813.

Dosenbach NU, Visscher KM, Palmer ED, et al. 2006. A core system for the implementation of task sets. Neuron 50:799–812.

Dougherty DD, Baer L, Cosgrove GR, et al. 2002. Prospective long-term follow-up of 44 patients who received cingulotomy for treatment-refractory obsessive-compulsive disorder. Am J Psychiatry 159:269–275.

Friston KJ, Holmes L, Worsely KJ, Poline JB, Firth CD, Frackowiak RSJ. 1995. Statistical parametric maps in functional imaging: a general linear approach. Hum Brain Mapp 2:189–210.

Ghahremani A, Rastogi A, Lam S. 2015. The role of right anterior insula and salience processing in inhibitory control. J Neurosci 35:3291–3292.

Gluth S, Rieskamp J, Buchel C. 2012. Deciding when to decide: time-variant sequential sampling models explain the emergence of value-based decisions in the human brain. J Neurosci 32:10686–10698.

Greicius MD, Krasnow B, Reiss AL, Menon V. 2003. Functional connectivity in the resting brain: a network analysis of the default mode hypothesis. Proc Natl Acad Sci U S A 100:253–258.

Grinband J, Hirsch J, Ferrera VP. 2006. A neural representation of categorization uncertainty in the human brain. Neuron 49:757–763.

Gu X, Hof PR, Friston KJ, Fan J. 2013. Anterior insular cortex and emotional awareness. J Comp Neurol 521:3371–3388.

Ham T, Leff A, de Boissezon X, Joffe A, Sharp DJ. 2013. Cognitive control and the salience network: an investigation of error processing and effective connectivity. J Neurosci 33:7091–7098.

Handwerker DA, Ollinger JM, D'Esposito M. 2004. Variation of BOLD hemodynamic responses across subjects and brain regions and their effects on statistical analyses. NeuroImage 21:1639–1651.

Ho TC, Brown S, Serences JT. 2009. Domain general mechanisms of perceptual decision making in human cortex. J Neurosci 29:8675–8687.

Holroyd CB, Yeung N. 2012. Motivation of extended behaviors by anterior cingulate cortex. Trends Cogn Sci 16:122–128.

Ide JS, Shenoy P, Yu AJ, Li CS. 2013. Bayesian prediction and evaluation in the anterior cingulate cortex. J Neurosci 33:2039–2047.

Kennerley SW, Walton ME, Behrens TE, Buckley MJ, Rushworth MF. 2006. Optimal decision making and the anterior cingulate cortex. Nat Neurosci 9:940–947.

Kosillo P, Smith AT. 2010. The role of the human anterior insular cortex in time processing. Brain Struct Funct 214:623–628.

Krebs RM, Boehler CN, Roberts KC, Song AW, Woldorff MG. 2012. The involvement of the dopaminergic midbrain and cortico-striatal-thalamic circuits in the integration of reward prospect and attentional task demands. Cereb Cortex 22:607–615.

Lamichhane B, Adhikari BM, Dhamala M. 2016. The activity in the anterior insulae is modulated by perceptual decision-making difficulty. Neuroscience 327:79–94.

Lamichhane B, Dhamala M. 2015a. Perceptual decision-making difficulty modulates feedforward effective connectivity to the dorsolateral prefrontal cortex. Front Hum Neurosci 9:498.

Lamichhane B, Dhamala M. 2015b. The salience network and its functional architecture in a perceptual decision: an effective connectivity study. Brain Connect 5:362–370.

Landmann C, Dehaene S, Pappata S, Jobert A, Bottlaender M, Roumenov D, Le Bihan D. 2007. Dynamics of prefrontal and cingulate activity during a reward-based logical deduction task. Cereb Cortex 17:749–759.

Lewis JW, Beauchamp MS, DeYoe E. 2000. A comparision of visual and auditory motion processing in human cerebral cortex. Cereb Cortex 10:873–888.

Medford N, Critchley HD. 2010. Conjoint activity of anterior insular and anterior cingulate cortex: awareness and response. Brain Struct Funct 214:535–549.

Menon V. 2015. Salience network. In: Toga AW (ed.) *Brain Mapping: An Encyclopedic Reference*, vol. 2. San Diego, CA: Academic Press, Elsevier; pp. 597–611.

Menon V, Uddin LQ. 2010. Saliency, switching, attention and control: a network model of insula function. Brain Struct Funct 214:655–667.

Mesulam MM, Mufson EJ. 1982a. Insula of the old world monkey. II: afferent cortical output and comments on function. J Comp Neurol 212:23–37.

Mesulam MM, Mufson EJ. 1982b. Insula of the world monkey. III: efferent cortical output and comments on function J Comp Neurol 212:38–52.

Metzler-Baddeley C, Jones DK, Steventon J, Westacott L, Aggleton JP, O'Sullivan MJ. 2012. Cingulum microstructure predicts cognitive control in older age and mild cognitive impairment. J Neurosci 32:17612–17619.

Nee DE, Kastner S, Brown JW. 2011. Functional heterogeneity of conflict, error, task-switching, and unexpectedness effects within medial prefrontal cortex. NeuroImage 54:528–540.

Paus T. 2001. Primate anterior cingulate cortex: white motor control drive and cognition interface. Nat Rev Neurosci 2:417–424.

Picard N, Strick PL. 1996. Motor area of the medial wall: a review of their location and functional activation. Cereb Cortex 6:342–353.

Ploran EJ, Nelson SM, Velanova K, Donaldson DI, Petersen SE, Wheeler ME. 2007. Evidence accumulation and the moment of recognition: dissociating perceptual recognition processes using fMRI. J Neurosci 27:11912–11924.

Pons F, Lewkowicz DJ. 2014. Infant perception of audio-visual speech synchrony in familiar and unfamiliar fluent speech. Acta Psychol 149:142–147.

Quilodran R, Rothe M, Procyk E. 2008. Behavioral shifts and action valuation in the anterior cingulate cortex. Neuron 57:314–325.

Raichle ME, MacLeod AM, Snyder AZ, Powers WL, Gusnard DA, Shulman GL. 2001. A default mode of brain function. Proc Natl Acad Sci U S A 98:676–682.

Roebroeck A, Formisano E, Goebel R. 2011. The identification of interacting networks in the brain using fMRI: model selection, causality and deconvolution. NeuroImage 58:296–302.

Rushworth MF, Behrens TE, Rudebeck PH, Walton ME. 2007. Contrasting roles for cingulate and orbitofrontal cortex in decisions and social behaviour. Trends Cogn Sci 11:168–176.

Rushworth MF, Walton ME, Kennerley SW, Bannerman DM. 2004. Action sets and decisions in the medial frontal cortex. Trends Cogn Sci 8:410–417.

Rushworth MF, Hadland KA, Gaffan D, Passingham RE. 2003. The effect of cingulate cortex lesions on task switching and working memory. J Cogn Neurosci 15:338–353.

Saper CB. 2002. The central autonomic nervous system: conscious visceral perception and autonomic pattern generation. Annu Rev Neurosci 25:433–469.

Seeley WW, Menon V, Schatzberg AF, et al. 2007. Dissociable intrinsic connectivity networks for salience processing and executive control. J Neurosci 27:2349–2356.

Shenhav A, Botvinick MM, Cohen JD. 2013. The expected value of control: an integrative theory of anterior cingulate cortex function. Neuron 79:217–240.

Singer T, Critchley HD, Preuschoff K. 2009. A common role of insula in feelings, empathy and uncertainty. Trends Cogn Sci 13:334–340.

Sridharan D, Levitin DJ, Menon V. 2008. A critical role for the right fronto-insular cortex in switching between central-executive and default-mode networks. Proc Natl Acad Sci U S A 105:12569–12574.

Srinivasan L, Asaad WF, Ginat DT, Gale JT, Dougherty DD, Williams ZM, et al. 2013. Action initiation in the human dorsal anterior cingulate cortex. PLoS One 8:e55247.

Sterzer P, Kleinschmidt A. 2010. Anterior insula activations in perceptual paradigms: often observed but barely understood. Brain Struct Funct 214:611–622.

Stevenson RA, Wallace MT. 2013. Multisensory temporal integration: task and stimulus dependencies. Exp Brain Res 227:249–261.

Stuss DT, Alexander MP, Shallice T, et al. 2005. Multiple frontal systems controlling response speed. Neuropsychologia 43:396–417.

Taylor PC, Nobre AC, Rushworth MF. 2007. Subsecond changes in top down control exerted by human medial frontal cortex during conflict and action selection: a combined transcranial magnetic stimulation electroencephalography study. J Neurosci 27:11343–11353.

Thielscher A, Pessoa L. 2007. Neural correlates of perceptual choice and decision making during fear-disgust discrimination. J Neurosci 27:2908–2917.

Touroutoglou A, Hollenbeck M, Dickerson BC, Feldman Barrett L. 2012. Dissociable large-scale networks anchored in the

right anterior insula subserve affective experience and attention. NeuroImage 60:1947–1958.
Tregellas JR, Davalos DB, Rojas DC. 2006. Effect of task difficulty on the functional anatomy of temporal processing. NeuroImage 32:307–315.
Valdes-Sosa PA, Roebroeck A, Daunizeau J, Friston K. 2011. Effective connectivity: influence, causality and biophysical modeling. NeuroImage 58:339–361.
van den Heuvel MP, Mandl RC, Kahn RS, Hulshoff Pol HE. 2009. Functionally linked resting-state networks reflect the underlying structural connectivity architecture of the human brain. Hum Brain Mapp 30:3127–3141.
van Eijk RLJ, Kohlrausch A, Juola JF, van de Par S. 2008. Audiovisual synchrony and temporal order judgments: effects of experimental method and stimulus type. Percept Psychophys 70:955–968.
van Wassenhove V, Grant KW, Poeppel D. 2007. Temporal window of integration in auditory-visual speech perception. Neuropsychologia 45:598–607.
Vatakis A, Spence C. 2006. Audiovisual synchrony perception for speech and music assessed using a temporal order judgment task. Neurosci Lett 393:40–44.
Venkatraman V, Rosati AG, Taren AA, Huettel SA. 2009. Resolving response, decision, and strategic control: evidence for a functional topography in dorsomedial prefrontal cortex. J Neurosci 29:13158–13164.
Walton ME, Devlin JT, Rushworth MF. 2004. Interactions between decision making and performance monitoring within prefrontal cortex. Nat Neurosci 7:1259–1265.
Wiech K, Lin CS, Brodersen KH, Bingel U, Ploner M, Tracey I. 2010. Anterior insula integrates information about salience into perceptual decisions about pain. J Neurosci 30:16324–16331.
Williams ZM, Bush G, Rauch SL, Cosgrove GR, Eskandar EN. 2004. Human anterior cingulate neurons and the integration of monetary reward with motor responses. Nat Neurosci 7:1370–1375.
Woolgar A, Hampshire A, Thompson R, Duncan J. 2011. Adaptive coding of task-relevant information in human frontoparietal cortex. J Neurosci 31:14592–14599.
Wu GR, Liao W, Stramaglia S, Ding JR, Chen H, Marinazzo D. 2013. A blind deconvolution approach to recover effective connectivity brain networks from resting state fMRI data. Med Image Anal 17:365–374.
Zampini M, Guest S, Shore DI, Spence C. 2005. Audio-visual simultaneity judgments. Percept Psychophys 67:531–544.
Zampini M, Shore DI, Spence C. 2003. Audiovisual temporal order judgments. Exp Brain Res 152:198–210.
Zysset S, Wendt CS, Volz KG, Neumann J, Huber O, von Cramon DY. 2006. The neural implementation of multi-attribute decision making: a parametric fMRI study with human subjects. NeuroImage 31:1380–1388.

Address correspondence to:
Bhim M. Adhikari
Department of Physics and Astronomy
Georgia State University
1 Park Place, Room No. 431
Atlanta, GA, 30303

E-mail: badhikari1@gsu.edu